Applied Catalysis A: General 392 (2011) 1–10

Contents lists available at ScienceDirect

Applied Catalysis A: General

journal homepage: www.elsevier.com/locate/apcata

# Synthesis and characterization of Pt/Fe–Zr catalysts for the CO selective oxidation

Martin Schmal[a,*], Ricardo Scheunemann[a], Nielson F.P. Ribeiro[a], Jose Fernando Bengoa[b], Sergio Gustavo Marchetti[b]

[a] NUCAT/COPPE/UFRJ, Centro de Tecnologia, Bloco G, sala 128, CEP 21945-970 Rio de Janeiro/RJ, Brazil
[b] CINDECA-UNLP, CONICET-CICPBA, Rua 47 n° 257, CEP 1900 La Plata, Argentina

ARTICLE INFO

*Article history:*
Received 18 June 2010
Received in revised form
18 September 2010
Accepted 24 September 2010
Available online 1 October 2010

*Keywords:*
Mixed oxides
Iron–zirconia
Iron catalyst
Mössbauer
SELOX reaction

ABSTRACT

Catalysts of Pt on $Fe_2O_3$ and mixed oxides $Fe_xZr_{(1-x)}O_2$ were prepared for the selective CO + $H_2$ oxidation. X-ray diffraction and Mössbauer spectroscopy showed α-$Fe_2O_3$ in pure support, a solid solution for $x = 0.25$ and mixed oxides with segregated phases for higher "$x$" values. Mössbauer results showed also that with increasing the Zr content $Zr^{4+}$ ions substitute the $Fe^{3+}$ ions in the α-$Fe_2O_3$ lattice, and also $Fe^{3+}$ ions diffusing into the zirconia lattice. The $Pt/Fe_{0.25}Zr_{0.75}O_2$(p) exhibited only $Fe^{3+}$ inside the $ZrO_2$ lattice. After reduction, $Fe_3O_4$ was found in the catalysts, which decreased with increasing zirconium loading. It is interesting to note that the corresponding precursor presents 83% of $Fe^{3+}$ located in the $ZrO_2$ lattice and the remaining 17% corresponds to hematite.

Catalytic tests for the preferential oxidation of CO containing $H_2$ showed a maximum CO conversion at different temperatures after reaching total oxygen conversion. The CO conversion decreased with increasing iron content in the mixed oxide. The $Pt/Fe_2O_3$ catalyst is the most active compared to the other Pt/mixed oxide and $Pt/ZrO_2$. Results showed the following order: $Pt/Fe_2O_3$(c) > $Pt/Fe_{0.75}Zr_{0.25}O_2$(c) > $Pt/Fe_{0.25}Zr_{0.75}O_2$(c) > $Pt/ZrO_2$. The $Pt/Fe_{0.25}Zr_{0.75}O_2$(c) presented high selectivity (56%) at 90 °C and is 2-fold higher compared to the $Pt/Fe_2O_3$ and $Pt/ZrO_2$ catalyst.


## 1. Introduction

It is well known that the low temperature proton-exchange membrane fuel cells (PEMCF) are extremely sensitive to low levels of carbon monoxide (50 ppm). As a consequence, the CO should be eliminated from the feed, avoiding poisoning of the metal. Among the current methods the selective oxidation of CO (PROX) seems to be the most economic and efficient approach. This reaction has been studied using different supports (silica, alumina and titania) and noble metals (Pt, Pd, Ru, Rh and Au) as catalysts [1–6]. Other types of solids used in the PROX reaction were ceria or ceria–zirconia supported transition metal (Cu, Co, Ni) catalysts [7]. On $CeO_2$ support the redox cycle Ce(III)–Ce(II) is easy and the oxygen mobility is facilitated. As a result, such oxides are able to absorb reversibly oxygen [8]. However, catalysts like CuO–$CeO_2$ are susceptible to the presence of water vapor and carbon dioxide [9]. Considering that for this reaction a redox cycle is important and that the cycle Fe(III)–Fe(II) can occur in an easy way (α-$Fe_2O_3 \leftrightarrow Fe_3O_4$), mixed oxides like $Fe_2O_3$–$ZrO_2$ could be interesting supports for noble metal catalysts to be used in the PROX reaction.

These mixed oxides have had important industrial applications in isomerization of hydrocarbons, hydrogenation of carbon monoxide [10–13] and dehydrogenation of ethylbenzene [14]. The addition of $Fe_2O_3$ increases the stability of zirconia catalysts [10] and zirconia increases the activity of the $Fe_2O_3$, stabilizing the $Fe^{3+}$ cations during the reduction [13]. Popovic et al. [14] prepared solid solutions in the thermodynamically stable $m$-$ZrO_2$-α-$Fe_2O_3$ system, using the coprecipitation method with $ZrO(NO_3)_2{\cdot}2H_2O$ and $Fe(NO_3)_3{\cdot}9H_2O$ as precursors salts in solution with different molar ratios. Calcination was carried out at several temperatures up to 1100 °C. The incorporation of $Fe^{3+}$ produced an asymmetrical distortion in the apex of the crystallites of $m$-$ZrO_2$. Likewise, Stefanic et al. [15] followed the phase change of $Fe_2O_3$–$ZrO_2$ system during the calcination at different temperatures (500, 600, 800 and 1100 °C). A solid solution was observed at 600 °C with $Fe_2O_3$ loadings up to 30 mol%, which crystallized in a metastable phase. It stabilizes as a cubic phase due to the formation of oxygen vacancies in the apexes of zirconia. These vacancies are associated to the $Fe^{3+}$ ions with a smaller ionic size than $Zr^{4+}$. The stabilization of cubic zirconia depends on the amount of $Fe^{3+}$ ions incorporated in the lattice of zirconia and also on the preparation conditions.

Following these ideas, the aim of the present work was to prepare $Pt/Fe_xZr_{(1-x)}O_2$ ($x = 0.25$, 0.5, 0.75) catalysts and comparing with $Pt/Fe_2O_3$ and $Pt/ZrO_2$ for the PROX reaction. In order to explain the catalytic results, the supports and the catalysts

* Corresponding author. Fax: +55 21 25628360.
*E-mail address:* schmal@peq.coppe.ufrj.br (M. Schmal).

0926-860X/$ – see front matter © 2010 Elsevier B.V. All rights reserved.
doi:10.1016/j.apcata.2010.09.027

were characterized by X-ray diffraction, temperature programmed reduction, temperature programmed desorption and Mössbauer spectroscopy.

## 2. Experimental

### 2.1. Preparation

- Zirconia ($ZrO_2$) was prepared by calcination of ($ZrO(NO_3)\cdot 2H_2O$ (Aldrich) at 10 °C/min under airflow (120 mL/min) in a muffle with programmed temperature up to 500 °C, for 2 h and was used as reference in this study.
- Iron oxide ($Fe_2O_3$) was obtained by calcination of iron (III) nitrate (Vetec) in airflow (120 mL/min) at 500 °C (10 °C/min) for 2 h.
- The $Fe_xZr_{(1-x)}O_2$ oxides were prepared by co-precipitation using $ZrO(NO_3)_2\cdot 2H_2O$ and $Fe(NO_3)_3\cdot 9H_2O$ as precursors. A mixture of reagents at different molar Fe/Zr ratios was co-precipitated with 25% $NH_4OH$ in aqueous solution at pH 10.4. The resulting powders were dried for 12 h at 90 °C, calcined in airflow at 500 °C (2 °C/min) and kept for 2 h, as described in [14]. (Here *x* was codified as weight percentage). These oxides will be used as supports of Pt catalysts and were denoted as $Fe_xZr_{(1-x)}O_2$(s).
- Pt was incorporated using a solution of $H_2PtCl_6$ (Sigma) by incipient wetness impregnation. The samples were dried for 12 h at 90 °C and calcined in airflow (120 mL/min) at 500 °C (5 °C/min) for 2 h. The samples are the precursors of the catalysts and will be represented by the formula $Pt/Fe_xZr_{(1-x)}O_2$(p). Finally, the precursors were activated as will be described in Section 2.3, and the catalysts obtained will be denoted as $Pt/Fe_xZr_{(1-x)}O_2$(c).

### 2.2. Characterization of supports and catalysts

The characterizations were carried out using the following techniques:

- The chemical composition was determined by X-ray fluorescence (XRF) using a Rigaku spectrometer, RIX 3100 model apparatus.
- Specific surface area was measured by BET method, with $N_2$ adsorption measurements at liquid nitrogen temperature, using a Micromeritics ASAP 2000 apparatus. Before analysis, the sample was degassed for 24 h at 300 °C.
- X-ray powder diffraction patterns were recorded in a Rigaku miniflex X-ray diffractometer using CuKα radiation (30 kV and 15 mA). The diffractograms were recorded in the range of $2^\circ < 2\theta < 90^\circ$ with 0.05°/step.
- The precursors were reduced by temperature programmed reduction (TPR), carried out in a microflow reactor at atmospheric pressure. The samples were dehydrated at 250 °C under Ar flow before reduction. The temperature rises from room temperature to about 1000 °C at a heating rate of 10 °C/min, with a mixture of 1.59% $H_2$/Ar (v/v) (30 mL/min) flow. The outflow gases were analyzed by a thermal conductivity detector.
- Temperature programmed desorption of CO (named TPD-CO) was carried out using a QMS-200 (BALZER) mass spectrometer. Prior to CO adsorption, the samples (200 mg) were dried under He flow at 250 °C and cooled to room temperature. Then, reduced with a mixture of 10% $H_2$/He (30 mL/min). raising the temperature up to 500 °C (10 °C/min) and held for 30 min at this temperature. After cooling to room temperature in He flow at 30 mL/min, the sample was exposed to 10% CO/He flow for 1 h at room temperature. Physisorbed CO was removed by purging with He. Desorption started with He flow (30 mL/min) raising the temperature up to 220 °C (10 °C/min). Similar assay was done with the feed reaction (60% $H_2$ + 1% $O_2$ + 1% CO + balanced with He) (named TPD-feed) following the adsorption at room temperature and desorption with He flow, raising the temperature up to 220 °C. The ratios $m/e$ = 2, 12, 15, 16, 17, 18, 27, 28, 29, 32, and 44 were monitored for quantification.
- The Mössbauer spectra were obtained in transmission geometry with a 512-channel constant acceleration spectrometer. A source of $^{57}$Co in Rh matrix of nominally 50 mCi was used. Velocity calibration was performed against a 12 μm-thick α-Fe foil. All isomer shifts ($\delta$) mentioned in this paper are referred to this standard. The temperature of −243 °C was obtained using a Displex DE-202 Closed Cycle Cryogenic System. The Mössbauer spectra were evaluated using a commercial program with constraints named Recoil [16]. Lorentzian lines were considered with equal widths for each spectrum component. The spectra were folded to minimize geometric effects. The spectra of the reduced samples were obtained in the activation atmosphere using a cell specially built for this purpose to be used inside the cryogenic system [17].

### 2.3. Catalytic tests

The catalytic tests for the CO selective oxidation (PROX) were measured in a continuous flow fixed-bed U-shaped reactor, under atmospheric pressure. Effluent gases were analyzed by gas chromatography (VARIAN CP3800) equipped with a CP-PoraBOND Q column. The reaction was studied from 30 up to 220 °C, measuring the CO and $O_2$ conversions at different temperatures. The catalytic experiments were performed with 100 mg sample, using a feed composition of 1% CO, 1% $O_2$, 60% $H_2$ in He with a total flow rate of 100 mL/min. Priori the samples were dehydrated at 250 °C (10 °C/min) for 30 min using He (30 mL/min), reduced with a mixture of 10% $H_2$/He (30 mL/min) at 10 °C/min up to 500 °C and kept for 30 min at this temperature. The CO and $O_2$ conversions and the $CO_2$ selectivity were defined as follows:

$$\text{CO conversion } (\%) = \frac{[\text{CO}]_{\text{in}} - [\text{CO}]_{\text{out}}}{[\text{CO}]_{\text{in}}} \times 100 \quad (1)$$

$$\text{O}_2 \text{ conversion } (\%) = \frac{[\text{O}_2]_{\text{in}} - [\text{O}_2]_{\text{out}}}{[\text{O}_2]_{\text{in}}} \times 100 \quad (2)$$

$$\text{CO}_2 \text{ selectivity } (\%) = \frac{0.5 \times ([\text{CO}]_{\text{in}} - [\text{CO}]_{\text{out}})}{[\text{O}_2]_{\text{in}} - [\text{O}_2]_{\text{out}}} \times 100 \quad (3)$$

For comparison the activity was obtained at isoconversion (at low conversion) and at low temperature (70 °C).

## 3. Results and discussion

### 3.1. X-ray fluorescence (XRF) and surface area (BET)

The chemical compositions of the precursors are shown in Table 1. As it can be seen, the platinum content in the samples is close to the nominal value. However, the chemical compositions for the oxide samples are slightly different from the nominal values, which can be attributed to loss of material during the filtration and washing steps.

The textural analysis was carried out by $N_2$ physisorption using the BET method and the results are shown in Table 1. The $Pt/ZrO_2$ catalyst presented a surface area of 57 $m^2$/g. The $Pt/Fe_2O_3$(p) sample presented low specific surface area (14 $m^2$/g) when compared to reported values of Tripathi et al. [18] and Qiu et al. [19], which used different precursors. Their surface areas were 41 and 50 $m^2$/g after calcination at 400 and 350 °C, respectively. Menezes et al. [20] obtained less than 10 $m^2$/g after calcination at several temperatures (200, 300, 400, 500 and 600 °C), using the same precursor salts as here. Shaheen [21] used a $Fe(OH)_2\cdot FeCO_3$ like precursor and obtained specific areas of 51, 40 and 32 $m^2$/g, after calcination at 350, 550 and 750 °C, respectively.

**Table 1**
Chemical composition, $N_2$ physisorption and TPR quantification results of the catalyst and precursors.

| Samples | Nominal content (%) | | | Real content (%) | | | | BET ($m^2/g_{cat}$) | Reduction degree (%) |
|---|---|---|---|---|---|---|---|---|---|
| | Pt | $Fe_2O_3$ | $ZrO_2$ | Pt | $Fe_2O_3$ | $ZrO_2$ | $Cl^-$ | | |
| $Fe_2O_3$(s) | – | – | – | – | – | – | – | – | 88.8[a], 68.2[b] |
| $Fe_{0.25}Zr_{0.75}O_2$(s) | – | – | – | – | – | – | – | – | 95.4[c] |
| $Fe_{0.5}Zr_{0.5}O_2$(s) | – | – | – | – | – | – | – | – | 96.1[c] |
| $Fe_{0.75}Zr_{0.25}O_2$(s) | – | – | – | – | – | – | – | – | 28.6[c] |
| $Pt/ZrO_2$ | 1 | – | 100 | 1.06 | – | 96.2 | – | 57 | 50.9[d] |
| $Pt/Fe_{0.25}Zr_{0.75}O_2$(p) | 1 | 24.75 | 74.25 | 1.0 | 22.5 | 75.4 | 1.1 | 164 | 94.3[d] |
| $Pt/Fe_{0.5}Zr_{0.5}O_2$(p) | 1 | 49.50 | 49.50 | 1.1 | 44.8 | 52.1 | 2.0 | 75 | 49.4[d] |
| $Pt/Fe_{0.75}Zr_{0.25}O_2$(p) | 1 | 74.25 | 24.75 | 0.9 | 70.1 | 27.6 | 1.4 | 68 | 51.4[d] |
| $Pt/Fe_2O_3$(p) | 1 | 99.00 | – | 1.1 | 98.4 | – | 0.5 | 14 | >100 |

[a] First peak reduction ($3Fe_2O_3 + H_2 \rightarrow 2Fe_3O_4 + H_2O$).
[b] Second peak reduction ($Fe_3O_4 + 4H_2 \rightarrow 3Fe + H_2O$).
[c] ($Fe_2O_3 + 3H_2 \rightarrow 2Fe + 3H_2O$).
[d] First peak reduction ($Pt^{4+} \rightarrow Pt^{\circ}$).

On the other hand, the specific surface areas of the $Pt/Fe_xZr_{(1-x)}O_2$(p) samples increased significantly depending of the molar compositions of zirconia, resulting in high specific surface areas (68–164 $m^2/g$) when compared to the literature. Wu et al. [11] prepared Fe–Zr mixed oxides using ferric chloride and zirconium tetrachloride salts. After drying at 110 °C and calcining at 700 °C the surface area was 49 $m^2/g$ with 80% zirconia.

### 3.2. X-ray powder diffraction

The XRD diffractograms of the supports and precursors are presented in Fig. 1A–E. Fig. 1A displays the diffractogram of $ZrO_2$(s) and $Pt/ZrO_2$(p). As shown the diffractograms present crystalline monoclinic structure represented in the lines at 24,31°, 28,39°, 31,53°, 34,39°, 40,90° (JCPDS 371484). The $Fe_2O_3$(s) and $Pt/Fe_2O_3$(p) sam-

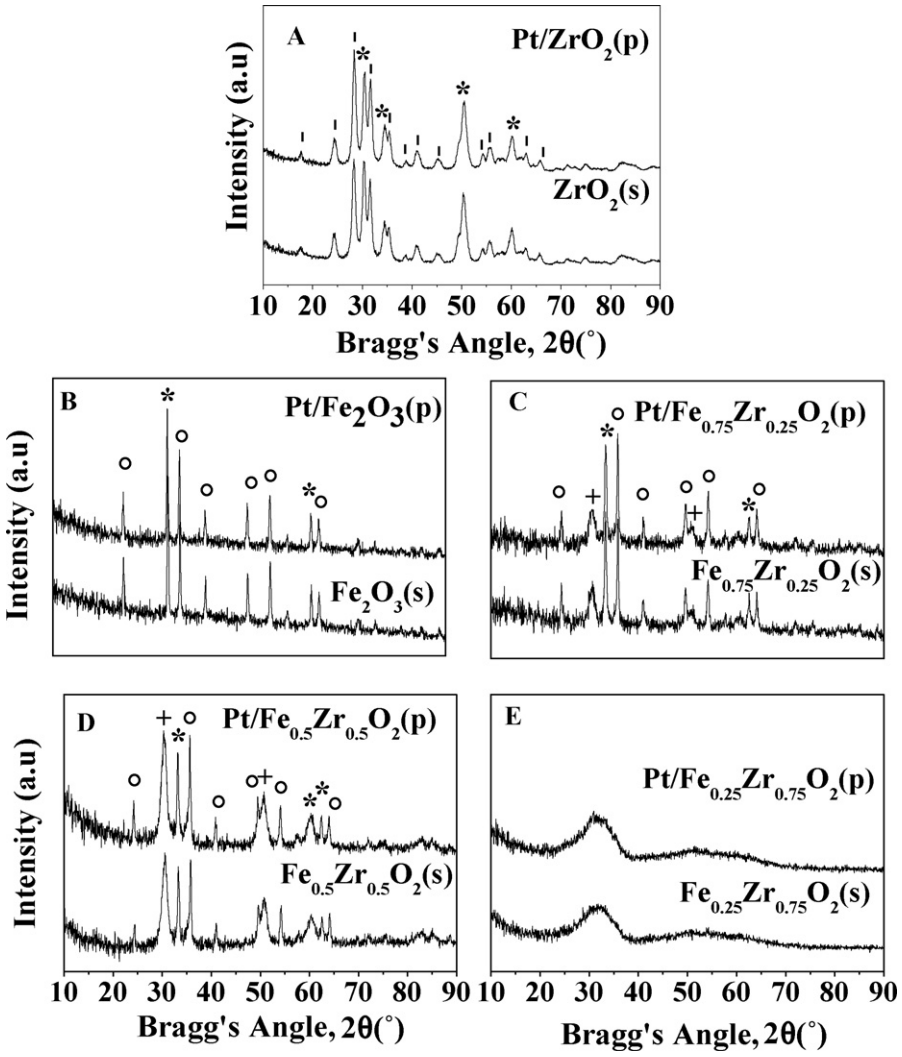


**Fig. 1.** X-ray diffraction patterns of the samples and its respective supports. (°) cubic $Fe_2O_3$, (*) hexagonal $Fe_2O_3$ and (+) cubic or tetragonal $ZrO_2$ and (I) monoclinic $ZrO_2$.

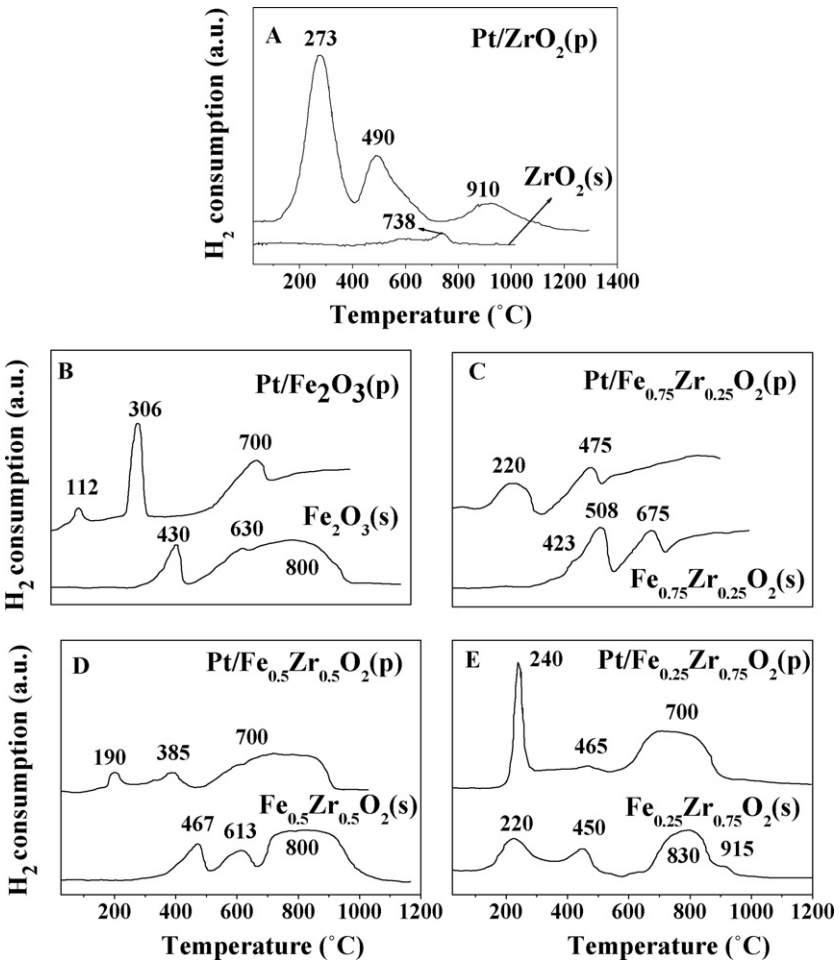


**Fig. 2.** TPR profiles of the different samples.

ples (Fig. 1B) displayed sharp and symmetric diffraction lines, indicating good crystallinity. Both presented crystalline phases of α-$Fe_2O_3$ with diffraction lines at 2$\theta$: at 24.37°, 33.54°, 35.81°, 41.03°, 49.70°, 54.29°, 62.73° and 64.17° (JCPDS 33664).

The diffractograms of the samples with 75% and 50% of iron oxide content and the related precursors are presented in Fig. 1C and D, showing α-$Fe_2O_3$ phase (JCPDS 33664), as well as $ZrO_2$ as tetragonal or cubic phase (JCPDS 27997), suggesting the formation of segregated phases. The zirconium oxide presented diffraction lines at 30.6° and 50.6°. On the other hand, the $Fe_{0.25}Zr_{0.75}O_2$(s) and Pt/$Fe_{0.25}Zr_{0.75}O_2$(p) samples (Fig. 1E) did not present well defined crystalline structures, instead a broad peak around 35°, can be observed. It suggests the presence of very small crystallites after calcination at 500 °C or formation of amorphous solids. It agrees with Stefanic et al. [15,22] results that found a similar diffraction pattern for a system with 30% iron and 70% zirconia. The intensity of this $ZrO_2$ phase decreases with increasing iron oxide content, in agreement with Stefanic et al. [15]. Taking into account that the diffraction patterns of cubic and tetragonal $ZrO_2$ are almost identical, and considering that in the present samples the diffraction lines assigned to $ZrO_2$ are very broad, it is not possible to distinguish between both phases. These results also agreed with Stefanic et al. [15]. Platinum was not observed in the diffractograms, indicating that this content is below the detection level [23].

### 3.3. Temperature programmed reduction

Reduction of the supports samples (s) and the precursors (p) with Pt after calcination are shown in Fig. 2A–E.

Fig. 2A shows the TPR profiles of $ZrO_2$ (bottom line) and the Pt/$ZrO_2$ catalyst (upper line). Zirconia is stable presenting only a small reduction peak at 738 °C with 5.4% of zirconia. This result is consistent with the literature, Bozo et al. [15], Querino et al. [16] and Dong et al. [17]. The Pt/$ZrO_2$ catalyst displayed the main peak at 273 °C with a small shoulder around 130 °C, a second peak at 490 °C and a third peak at 910 °C. The hydrogen consumption is higher than needed to the complete reduction of Pt oxide, in agreement with Souza et al. [18], which sustains the hypothesis that sub surfaces oxides species of zirconia at the interface can be reduced at lower temperature. Indeed, reduced Pt dissociates $H_2$ which migrates to the zirconia surface and facilitate their reduction. The first peak at 273 °C is associated to the reduction of $Pt^{4+} \rightarrow Pt^{\circ}$, while the reduction at higher temperature is attributed to the additional reduction of $Zr^{4+} \rightarrow Zr^{3+}$ promoted by metallic Pt at the surface. The small shoulder around 130 °C is probably attributed to the reduction of greater $PtO_2$ particles and at 930 °C the reduction of $ZrO_2$.

Fig. 2B shows the reduction profile of $Fe_2O_3$ (bottom line) indicating the reduction of $Fe_2O_3$ to $Fe_3O_4$ (Eq. (4)) in the first peak at 430 °C followed by the reduction of $Fe_3O_4$ to metallic iron $Fe^0$ (Eq. (5)) on the second broad peak between 500 and 950 °C, with maximum around 800 °C. The reduction degrees were calculated as shown in Table 1:

$$3Fe_2O_3 + H_2 \rightarrow 2Fe_3O_4 + H_2O \quad (4)$$

$$Fe_3O_4 + 4H_2 \rightarrow 3Fe + 4H_2O \quad (5)$$

For the mixed oxides the reduction was calculated based on the total reduction of iron oxide, according to Eq. (6).

$$Fe_2O_3 + 3H_2 \rightarrow 2Fe + 3H_2O \quad (6)$$

Souza et al. [25] observed reduction of hematite to magnetite in a first peak, followed by the formation of metallic iron. The first peak is exothermic, occurring around 300 °C, while the second peak occurs at higher temperature. Chen et al. [26] reported maximum reduction temperatures at 400 and 600 °C and Heidebrecht et al. [27] found reduction at temperatures around 400 as well as 700 °C. Likewise, Lin et al. [28] studying a similar system obtained peaks at 300 and 500 °C. Our results are consistent with the literature.

The reduction profile of the precursor $Pt/Fe_2O_3(p)$ is displayed in Fig. 2B (upper line) showing three peaks at 112, 306 and 700 °C. Comparing with the $Pt/ZrO_2$ catalyst it shows that the main peak shifted from 273 to 306 °C and the small shoulder to 112 °C and a second peak at 490 °C. The peak at 306 °C is attributed to the reduction of $PtO_2$ and a partial reduction of $Fe_2O_3$. Comparing with the reduction profile of $Fe_2O_3(s)$ it shows that the reduction of platinum oxide is facilitated by the reduction of Fe oxide at the interface. The second peak was shifted to lower temperature due to the catalytic effect of platinum on the reduction of iron oxide. Finally, the last peak of reduction is assigned to the reduction of the Fe oxide.

Samples with 75% and 50% iron (Fig. 2C and D) displayed similar reduction profiles and when compared to the iron oxide profiles, they exhibited three distinct maxima, which are shifted to higher temperatures. With increasing iron content these reduction peaks are also shifted to higher temperatures.

The reduction profiles of these precursors showed different shapes in the lower temperature range but very similar profiles to the supports at higher temperatures. It suggests the reduction of segregated phases of iron oxide at elevated temperatures. The reduction degrees are also similar to pure iron oxide, according to Table 1. XRD results confirm that these precursors evidence the presence of a mixture of iron oxide and zirconium oxide with different crystalline structures and not a solid solution of Fe–Zr.

The $Fe_{0.25}Zr_{0.75}O_2(s)$ (Fig. 2E bottom line) presented a different reduction profile, displaying peaks at 220, 450 °C and a broad peak in the range from 650 to 950 °C. The last one may be related to reduction of iron oxide, according to Eqs. (4) and (5). The first peak at low temperature seems to be the reduction of the mixed oxide due to the formation of a solid solution, as observed by XRD.

The $Pt/Fe_{0.25}Zr_{0.75}O_2(p)$ (Fig. 2E upper line) shows a sharp reduction peak of platinum oxide at 240 °C. Besides, the reduction degree of this solid was higher than the other precursors. In consequence, the reduction of the mixed oxide occurs jointly with the platinum and iron species.

### 3.4. Temperature programmed desorptions of CO and the feed mixture

The TPD-feed on $Pt/ZrO_2$ presented desorption of CO at 93 °C, $CO_2$ and $H_2$ at 220 °C (not shown). However, with the addition of Fe the mixed oxide $Pt/Fe_{0.25}Zr_{0.75}O_2(c)$ displayed a large desorption peak of $CO_2$ at 195 °C, together with a small desorption of CO and no $H_2$ desorption (Fig. 3A). With increasing Fe content the $Pt/Fe_{0.5}Zr_{0.5}O_2(c)$ and $Pt/Fe_{0.75}Zr_{0.25}O_2(c)$, the profiles changed, displaying small desorption peaks of CO and $CO_2$ and a note worthy high $H_2$ desorption peak above 200 °C, as shown in Fig. 3B.

Table 2 presents quantitatively the desorbed amounts of CO, $CO_2$ and $H_2$ after TPD-feed for all catalysts. The $Pt/Fe_{0.25}Zr_{0.75}O_2(c)$ desorbed about 50 times more $CO_2$ and 7 times more CO than $Pt/Fe_2O_3(c)$.

On the other hand, the CO and $CO_2$ desorption values of $Pt/Fe_{0.5}Zr_{0.5}O_2(c)$ and $Pt/Fe_{0.75}Zr_{0.25}O_2(c)$ were similar, decreasing with higher Fe content. The desorbed $CO_2$ and CO values are 5–10 times lower than for the $Pt/Fe_{0.25}Zr_{0.75}O_2(c)$ sample. Noteworthy is the $H_2$ desorption for $Pt/Fe_{0.5}Zr_{0.5}O_2(c)$ and for $Pt/Fe_{0.75}Zr_{0.25}O_2(c)$. The CO desorption corresponds to the irreversible and preferential adsorption on $Pt^\circ$ sites. These results suggest not only adsorption on metallic $Pt^\circ$ but probably at the $Pt^\circ/Fe^{3+}$ interface, since $Fe_2O_3$ does not adsorb CO. The adsorption at the interface decreases with increasing iron content.

**Table 2**
Quantification of desorbed species on TPD of feed reaction.

| Catalysts | Desorption of CO ($\mu$mol CO/$g_{cat}$) | Desorption of $CO_2$ ($\mu$mol $CO_2$/$g_{cat}$) | Desorption of $H_2$ ($\mu$mol/$g_{cat}$) |
|---|---|---|---|
| 1% $Pt/ZrO_2$ | 6.1[a] | 57.1 | 28.7 |
| $Pt/Fe_{0.25}Zr_{0.75}O_2(c)$ | 7.3[a] | 132.2 | – |
| $Pt/Fe_{0.5}Zr_{0.5}O_2(c)$ | 1.6[a] | 5.0 | 17.2 |
| $Pt/Fe_{0.75}Zr_{0.25}O_2(c)$ | 1.5[a] | 10.6 | 104.7 |
| $Pt/Fe_2O_3(c)$ | 1.0[a] | 3.2 | 9.7 |

[a] $m/e = 28$ from $CO_2$.

The formation of $CO_2$ is probably due to the fact that CO is decomposed on $Pt^\circ$ according to the *Bouduard* reaction. However, the enormous amount of $CO_2$ released from the $Pt/Fe_{0.25}Zr_{0.75}O_2(c)$ requires an additional explanation. It suggests that adsorbed CO may react with the oxygen of the lattice, producing $CO_2$ and oxygen vacancies, according to the reaction:

$$CO_{(ads)} + [O]_L \rightarrow CO_{2(g)} + [\,]_{(vacancies)}$$

The TPD-feed results showed also an unexpected great amount of $H_2$ released on the $Pt/Fe_{0.75}Zr_{0.25}O_2(c)$ catalyst. Probably $H_2$ migrated or spilt over from the metal to the mixed oxide depending on the Fe content. It also justifies the $H_2$ oxidation, which is greatly favored on the $Pt/Fe_{0.75}Zr_{0.25}O_2(c)$ catalyst, as observed on the catalytic tests. Therefore the $O^-$ species will promote the CO and $H_2$ oxidation, in accordance with Smit et al. [29]. Thus, from the TPD results one can suggest:

a. The CO adsorption occurs on the metal and at the interface of $Pt^\circ/Fe^{3+}$.
b. These mixed oxides present vacancies, depending of the Fe content, promoting the CO oxidation at low temperatures.
c. The Pt/mixed oxides interfaces promote the migration or spill over of $H_2$ to the support, depending on the Fe content.

### 3.5. Mössbauer spectroscopy

Fig. 4 shows the Mössbauer spectra of $Pt/Fe_2O_3(p)$ and $Pt/Fe_xZr_{(1-x)}O_2(p)$ at room temperature and the hyperfine parameters are listed in Table 3.

The hyperfine parameters of $Pt/Fe_2O_3(p)$ showed the presence of only one iron species: $\alpha$-$Fe_2O_3$ [30] (Fig. 4). The spectra of $Pt/Fe_{0.25}Zr_{0.75}O_2(p)$ and $Pt/Fe_{0.5}Zr_{0.5}O_2(p)$ at 25 °C were fitted with one doublet and one sextet. The hyperfine parameters of the sextet are typical of $\alpha$-$Fe_2O_3$. However, the values of the hyperfine magnetic field are diminished significantly in comparison with the value of hematite "bulk". This effect can be attributed to:

- small size of $\alpha$-$Fe_2O_3$ crystallites, produced by the presence of zirconium oxide. The existence of small particles would decrease the hyperfine magnetic field due to the phenomenon named collective magnetic excitations [31].
- the presence of $Zr^{4+}$ ions substituting isomorphically $Fe^{3+}$ ions in the $\alpha$-$Fe_2O_3$ lattice, since this substitution could also cause a decrease in the hyperfine magnetic field [22].

On the other hand, the doublet could be attributed to superparamagnetic $\alpha$-$Fe_2O_3$ (extremely small crystals) or paramagnetic $Fe^{3+}$

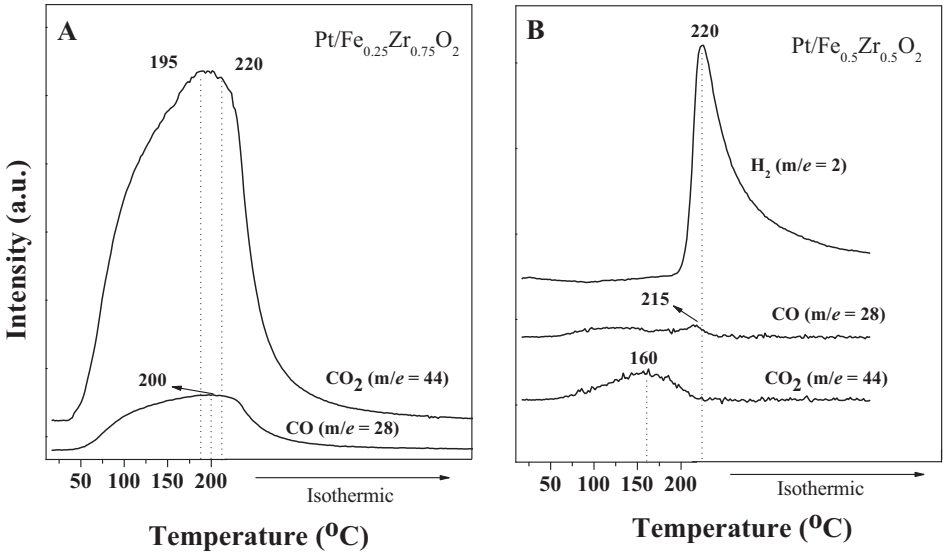


**Fig. 3.** TPD of reaction feed mixture 1% CO, 1%$O_2$, 60% $H_2$, He. (A) $Pt/Fe_{0.25}Zr_{0.75}O_2$ and (B) $Pt/Fe_{0.5}Zr_{0.5}O_2$.

**Table 3**
Mössbauer parameters of the precursors at 25 °C.

| Species | Parameters | $Pt/Fe_2O_3$(p) | $Pt/Fe_{0.75}Zr_{0.25}O_2$(p) | $Pt/Fe_{0.5}Zr_{0.5}O_2$(p) | $Pt/Fe_{0.25}Zr_{0.75}O_2$(p) |
|---|---|---|---|---|---|
| $\alpha$-$Fe_2O_3$ | $H$ (T) | 51.5 ± 0.1 | – | – | – |
| | $\delta$ (mm/s) | 0.37 ± 0.01 | – | – | – |
| | $2\varepsilon$ (mm/s) | −0.22 ± 0.01 | – | – | – |
| | % | 100 | – | – | – |
| $\alpha$-$Fe_2O_3$ with $Zr^{4+}$ | $H$ (T) | – | 50.6 ± 0.1 | 50.9 ± 0.1 | 50.5 ± 0.2 |
| | $\delta$ (mm/s) | – | 0.37 ± 0.01 | 0.37 ± 0.01 | 0.37 ± 0.02 |
| | $2\varepsilon$ (mm/s) | – | −0.22 ± 0.01 | −0.22 ± 0.01 | −0.27 ± 0.05 |
| | % | – | 74 ± 4 | 93 ± 1 | 17 ± 1 |
| $\alpha$-$Fe_2O_3$ with a higher $Zr^{4+}$ loading | $H$ (T) | – | 47.0 ± 0.8 | – | – |
| | $\delta$ (mm/s) | – | 0.35 ± 0.02 | – | – |
| | $2\varepsilon$ (mm/s) | – | −0.26 ± 0.04 | – | – |
| | % | – | 20 ± 4 | – | – |
| $Fe^{3+}$ in $ZrO_2$ | $\Delta$ | – | 1.12 ± 0.06 | 1.01 ± 0.06 | 1.07 ± 0.01 |
| | $\delta$ | – | 0.34 ± 0.04 | 0.38 ± 0.04 | 0.34 ± 0.01 |
| | % | – | 6 ± 1 | 7 ± 1 | 83 ± 1 |

$H$: hyperfine magnetic field in Tesla; $\delta$: isomer shift (all the isomer shifts are referred to α-Fe at 298 K); $2\varepsilon$: quadrupole shift; $\Delta$: quadrupole splitting.

ions located inside the lattice of $ZrO_2$ segregated. Considering that the value of quadrupole splitting ($\Delta$) is higher than that assigned to superparamagnetic $\alpha$-$Fe_2O_3$, the second hypothesis seems to be more plausible. In addition, the percentage of this doublet increases with the decreasing of Fe/Zr ratio, indicating that more $ZrO_2$ was segregated and, therefore, a greater amount of iron can be located inside the zirconia lattice [22,32].

In order to discern between these possibilities, the spectrum of $Pt/Fe_{0.25}Zr_{0.75}O_2$(p) at −243 °C was obtained (Fig. 4 and Table 4). This sample was selected to measure the spectrum at low temperature since it has the higher area of the doublet at room temperature. Therefore, the greater changes will be expected when the temperature decreases. Again, two interactions were used in the fitting: a sextuplet and a doublet, and their percentages are nearly identical to that obtained at room temperature. If very small $\alpha$-$Fe_2O_3$ crystallites would be present, a partial or total magnetic blocking would occur at −243 °C. In consequence, the percentage of the doublet would decrease and the area of the sextuplet would increase. Taking into account this analysis, the sextet could be assigned to $\alpha$-$Fe_2O_3$ with $Zr^{4+}$ ions substituting $Fe^{3+}$ ions, and the doublet to paramagnetic $Fe^{3+}$ ions located inside the $ZrO_2$ lattice. Due to the low percentage of $\alpha$-$Fe_2O_3$ with $Zr^{4+}$ ions (17 ± 1%) this species can not be detected by XRD. Therefore the $ZrO_2$ with $Fe^{3+}$ ions diffused inside its lattice originates the amorphous mixed oxide detected by XRD (Fig. 2).

**Table 4**
Mössbauer parameters of $Pt/Fe_{0.25}Zr_{0.75}O_2$(p) at −243 °C.

| Species | Parameters | $Pt/Fe_{0.25}Zr_{0.75}$ $O_2$(p) |
|---|---|---|
| $\alpha$-$Fe_2O_3$ with $Zr^{4+}$ | $H$ (T) | 52.8 ± 0.2 |
| | $\delta$ (mm/s) | 0.50 ± 0.02 |
| | $2\varepsilon$ (mm/s) | −0.17 ± 0.04 |
| | % | 22 ± 1 |
| $Fe^{3+}$ in $ZrO_2$ | $\Delta$ | 1.16 ± 0.01 |
| | $\delta$ | 0.46 ± 0.01 |
| | % | 78 ± 1 |

$H$: hyperfine magnetic field in Tesla; $\delta$: isomer shift (all the isomer shifts are referred to α-Fe at 298 K); $2\varepsilon$: quadrupole shift; $\Delta$: quadrupole splitting.

The hyperfine parameters for $Pt/Fe_{0.75}Zr_{0.25}O_2$(p) at 25 °C were obtained fitting with two sextets and one doublet. The assignment of the sextet with higher hyperfine magnetic field and the doublet are identical for samples $Pt/Fe_{0.25}Zr_{0.75}O_2$(p) and $Pt/Fe_{0.5}Zr_{0.5}O_2$(p). The second sextet showed a highly reduced hyperfine magnetic field value (47.0 T), in comparison with "bulk" hematite. If the hematite crystals are very small this signal could be assigned to the surface of these crystals [33]. However, this possibility can be excluded, because the value of $2\varepsilon$ is different to zero (value obtained for the surface layer of very small crystals of hematite). Instead, $2\varepsilon$ = −0.26 mm/s, a value almost identical to the hematite "bulk".

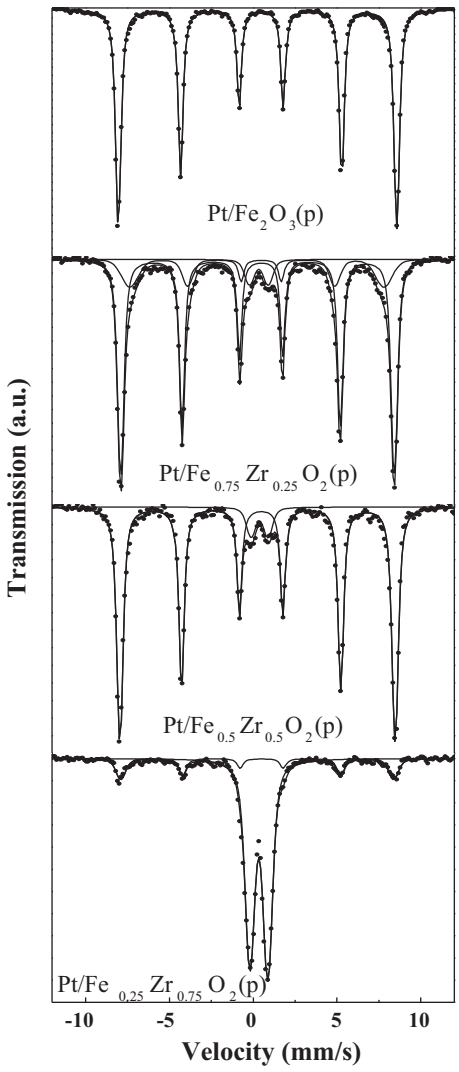


**Fig. 4.** Mössbauer spectra of $Pt/Fe_2O_3$(p), $Pt/Fe_{0.25}Zr_{0.75}O_2$(p), $Pt/Fe_{0.5}Zr_{0.5}O_2$(p) and $Pt/Fe_{0.75}Zr_{0.25}O_2$(p) at 25 °C.

For this reason, probably it is a second fraction of hematite in which there is a higher percentage of $Fe^{3+}$ ions isomorphically replaced by $Zr^{4+}$ (Fig. 5).

Mössbauer parameters obtained for the catalysts reduced at 500 °C and measured at room temperature in the same reducing atmosphere are listed in Table 5 and Fig. 6 shows the spectra. The catalysts $Pt/Fe_2O_3$(c), $Pt/Fe_{0.75}Zr_{0.25}O_2$(c) and $Pt/Fe_{0.5}Zr_{0.5}O_2$(c) showed two sextets whose hyperfine parameters can be assigned to $Fe^{3+}$ ions located in tetrahedral sites (sites A) and $Fe^{\text{“}2.5+\text{”}}$ ions located in octahedral sites (sites B) of $Fe_3O_4$, according to Vandenberghe et al. [30]. When the content of zirconium increased, two phenomena occur with the $Fe_3O_4$:

- the total amount of $Fe_3O_4$ decreased: 100% for $Pt/Fe_2O_3$(c); 90% for $Pt/Fe_{0.75}Zr_{0.25}O_2$(c); 78% for $Pt/Fe_{0.5}Zr_{0.5}O_2$(c) and 0% for $Pt/Fe_{0.25}Zr_{0.75}O_2$(c).
- the $Fe_3O_4$ is less stoichiometric since, the ratio of site B/site A populations, changes from 1.7 for $Pt/Fe_2O_3$(c), to 1.5 for $Pt/Fe_{0.75}Zr_{0.25}O_2$(c), and 1.4 for $Pt/Fe_{0.5}Zr_{0.5}O_2$(c). The value of this ratio for stoichiometric $Fe_3O_4$ is equal to 1.8 when it was determined by Mössbauer spectroscopy [30]. This means that the catalyst without zirconium has a nearly stoichiometric $Fe_3O_4$. On the other hand, when the zirconia content increases, the $Fe_3O_4$ is oxidized (higher percentage of $Fe^{3+}$ ions in comparison with to stoichiometric composition).

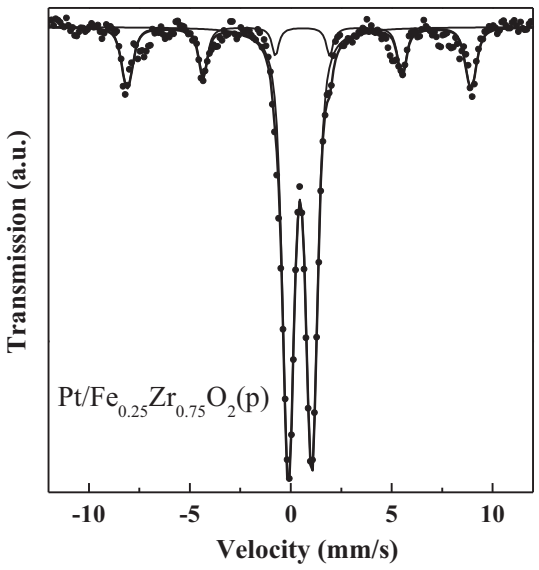


**Fig. 5.** Mössbauer spectra of $Pt/Fe_{0.25}Zr_{0.75}O_2$(p) at −243 °C.

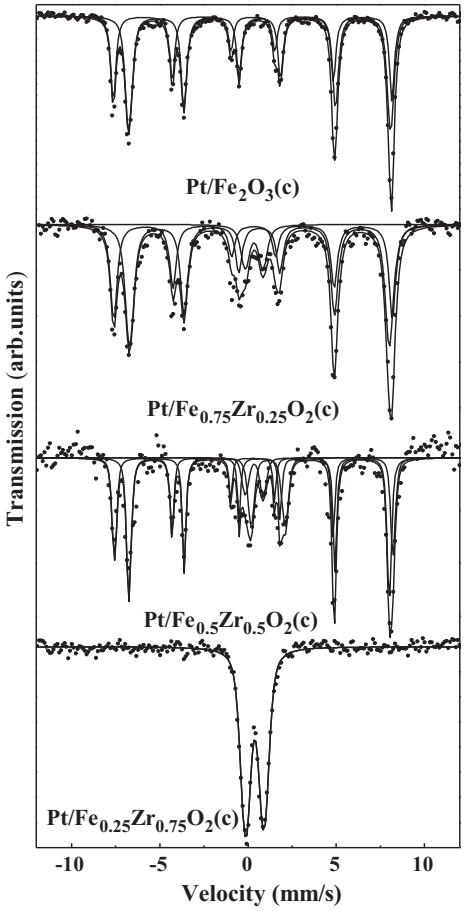


**Fig. 6.** Mössbauer spectra of samples $Pt/Fe_2O_3$(c), $Pt/Fe_{0.25}Zr_{0.75}O_2$(c), $Pt/Fe_{0.5}Zr_{0.5}O_2$(c) and $Pt/Fe_{0.75}Zr_{0.25}O_2$(c) in controlled atmosphere at 25 °C.

Moreover, in the sample $Pt/Fe_{0.75}Zr_{0.25}O_2$(c), the doublet can be attributed to unreduced superparamagnetic $\alpha$-$Fe_2O_3$ or paramagnetic $Fe^{3+}$ ions located inside the $ZrO_2$ lattice. Taking into account

**Table 5**
Mössbauer parameters of the catalysts at 25 °C.

| Species | Parameters | $Pt/Fe_2O_3(c)$ | $Pt/Fe_{0.75}Zr_{0.25}O_2(c)$ | $Pt/Fe_{0.5}Zr_{0.5}O_2(c)$ | $Pt/Fe_{0.25}Zr_{0.75}O_2(c)$ |
|---|---|---|---|---|---|
| $Fe^{3+}$ in tetrahedral sites (A) of $Fe_3O_4$ | $H$ (T) | 49.0 ± 0.1 | 49.0 ± 0.1 | 49.0 ± 0.1 | – |
| | $\delta$ (mm/s) | 0.27 ± 0.01 | 0.30 ± 0.02 | 0.29 ± 0.01 | – |
| | $2\varepsilon$ (mm/s) | −0.01 ± 0.01 | −0.02 ± 0.02 | 0.06 ± 0.02 | – |
| | % | 37 ± 1 | 36 ± 2 | 32 ± 2 | – |
| $Fe^{"2.5+"}$ in octahedral sites (B) of $Fe_3O_4$ | $H$ (T) | 46.0 ± 0.1 | 45.6 ± 0.1 | 45.8 ± 0.1 | – |
| | $\delta$ (mm/s) | 0.67 ± 0.01 | 0.65 ± 0.01 | 0.65 ± 0.01 | – |
| | $2\varepsilon$ (mm/s) | −0.01 ± 0.01 | 0.01 ± 0.01 | −0.02 ± 0.02 | – |
| | % | 63 ± 1 | 54 ± 2 | 46 ± 3 | – |
| $Fe^{2+}$ in $ZrO_2$ | $\Delta$ | – | – | 1.93 ± 0.08 | – |
| | $\delta$ | – | – | 1.14 ± 0.04 | – |
| | % | – | – | 14 ± 2 | – |
| $Fe^{3+}$ in $ZrO_2$ | $\Delta$ | – | 1.01 ± 0.09 | 1.0 ± 0.1 | 1.04 ± 0.01 |
| | $\delta$ | – | 0.34 ± 0.05 | 0.35 ± 0.08 | 0.38 ± 0.01 |
| | % | – | 10 ± 1 | 8 ± 2 | 100 |

$H$: hyperfine magnetic field in Tesla; $\delta$: isomer shift (all the isomer shifts are referred to α-Fe at 298 K); $2\varepsilon$: quadrupole shift; $\Delta$: quadrupole splitting.

**Table 6**
CO conversion and $CO_2$ selectivity at different temperatures and maximum conversion of oxygen.

| Temperature conversion/selectivity | 90 °C | | 110 °C | | 130 °C | | TOF ($h^{-1}$) |
|---|---|---|---|---|---|---|---|
| | $S_{CO_2}$ (%) | $X_{CO}$ (%) | $S_{CO_2}$ (%) | $X_{CO}$ (%) | $S_{CO_2}$ (%) | $X_{CO}$ (%) | |
| Catalysts | | | | | | | |
| 1% $Pt/ZrO_2$ | 22.5 | 2.4 | 16.8 | 6.6 | 16.7 | 28.1 | 2.17 |
| $Pt/Fe_{0.25}Zr_{0.75}O_2$ | 55.9 | 7.6 | 14.3 | 37.2 | 9.4 | 24.4 | 0.52 |
| $Pt/Fe_{0.5}Zr_{0.5}O_2$ | 6.7 | 17.3 | 5.7 | 14.8 | 4.9 | 12.6 | – |
| $Pt/Fe_{0.75}Zr_{0.25}O_2$ | 4.3 | 11.4 | 4.7 | 12.4 | 3.1 | 8 | 0.14 |
| $Pt/Fe_2O_3$ | 20.8 | 51.8 | 18 | 45.5 | 14 | 36.1 | 0.009 |

that the value of the quadrupole splitting is higher than that of superparamagnetic α-$Fe_2O_3$, and the previous discussion above the precursors, the second hypothesis seems to be more feasible in agreement with Stefanic et al. [22,32]. Besides, the percentage of the doublet detected is nearly identical to the value founded for the precursor; therefore, these $Fe^{3+}$ ions, located inside the $ZrO_2$ lattice, could not be reduced.

The $Pt/Fe_{0.5}Zr_{0.5}O_2(c)$ displayed two doublets: one of them with parameters characteristics of $Fe^{3+}$ assigned in the same way that in $Pt/Fe_{0.75}Zr_{0.25}O_2(c)$, but the second doublet has parameters characteristics of $Fe^{2+}$ in $ZrO_2$. The percentage of these two species exceeds the value of $Fe^{3+}$ ions that were inside the $ZrO_2$ lattice in the precursor. Therefore, during the reduction step a percentage of $Fe^{2+}$ diffuses inside the zirconia lattice.

The sample $Pt/Fe_{0.25}Zr_{0.75}O_2(c)$ only showed one doublet of $Fe^{3+}$, located in the $ZrO_2$ lattice. Here, it is interesting to note that the corresponding precursor presents 83% of $Fe^{3+}$ located in the $ZrO_2$ lattice and the remaining 17% corresponds to hematite. Since, any reduction was detected, can be speculated that during the reduction treatment the diffusion velocity of $Fe^{3+}$ inside the zirconia exceeded the reduction velocity, and therefore the $Fe^{3+}$ ions were kept within the zirconia lattice without any possibility of reduction.

### 3.6. Reaction tests

Fig. 7 and Table 6 show the influence of the temperature on CO conversion for the selective oxidation (PROX) reaction for all catalysts. Fig. 8 displays separately the CO and $O_2$ conversions and $CO_2$ selectivity for $Pt/Fe_2O_3(c)$, $Pt/Fe_{0.25}Zr_{0.75}O_2(c)$ and $Pt/ZrO_2(c)$. The maximum CO conversion is related to the maximum oxygen needed for the selective oxidation of the mixture $CO + O_2 + H_2$ to $CO_2$ and $H_2O$. The $Pt/ZrO_2$ presented 75% CO conversion at 150 °C. The $Pt/Fe_2O_3(c)$ presented a maximum CO conversion of 52%, however, at 90 °C and for 96% $O_2$ conversion. The $Pt/Fe_{0.25}Zr_{0.75}O_2(c)$ displayed maximum CO conversion of 37% for 100% oxygen conversion at 110 °C. With increasing temperature and iron content the CO conversion decreased.

Note worth is the selectivity as shown in Table 6. The $Pt/Fe_{0.25}Zr_{0.75}O_2(c)$ presented high selectivity (56%) at 90 °C and 2-fold higher compared to the $Pt/Fe_2O_3$ and $Pt/ZrO_2$ catalyst. It can be attributed to the defects in the structure and the presence of oxygen vacancies in the mixed oxide as well as the presence of interfacial $Pt/Fe^{3+}$ sites, according to Magnetic results.

Wootsch et al. [34] studied the PROX reaction on a $Pt/Ce_{0.15}Zr_{0.85}O_2$ catalyst and observed CO conversion of 57% at 100 °C, while Ayastuy et al. [23] reported CO conversion of 69% at 90 °C, agreeing with our $Pt/Fe_2O_3(c)$ results. Rossignol et al. [35] found 55% maximum CO conversion and 40% selectivity at 172 °C for $Au/ZrO_2$ catalyst. According to Rossignol et al. [35] the activity and selectivity depend on the redox capacity of the oxide support at the interface of metal/support and the presence of oxygen vacancies.

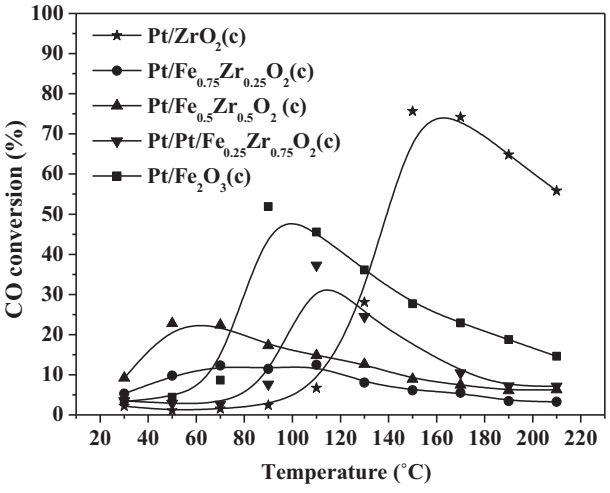


**Fig. 7.** CO conversion vs. temperature for samples $Pt/Fe_2O_3(c)$, $Pt/Fe_{0.25}Zr_{0.75}O_2(c)$, $Pt/Fe_{0.5}Zr_{0.5}O_2(c)$ and $Pt/Fe_{0.75}Zr_{0.25}O_2(c)$.

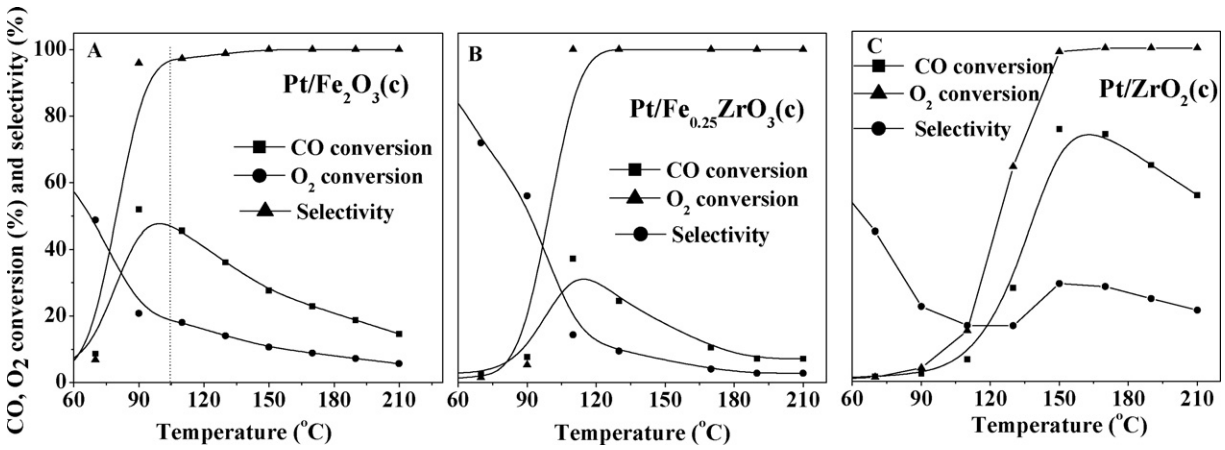


**Fig. 8.** CO and $O_2$ conversions and $CO_2$ selectivity vs. temperature for the $Pt/ZrO_2$; $Pt/Fe_{0.25}Zr_{0.75}O_2$(c) and $Pt/Fe_2O_3$(c) catalysts.

The activity (TOF) was determined under isoconversion (2–10%) at 70 °C and after CO chemisorption for all samples, as presented in Table 6. Results showed the following order: $Pt/Fe_2O_3(c) > Pt/Fe_{0.75}Zr_{0.25}O_2(c) > Pt/Fe_{0.25}Zr_{0.75}O_2(c) > Pt/ZrO_2$. These catalysts favored both CO and $H_2$ oxidation, even at low temperatures but not as sufficient as required to produce high CO conversion. Moreover, higher iron loading favored $H_2$ oxidation with increasing temperature, which is in accordance with TPD-feed results. Indeed, the mixed oxide supports increases the $H_2$ storage capacity in the structure and the CO coverage decreases at the metal and $Pt/Fe^{3+}$ interface [29].

This behavior may be explained considering the influence of different properties of these materials on the reaction mechanisms. Schubert et al. [36] observed that gold-based catalysts over inert supports (e.g. $Al_2O_3$, $SiO_2$ and MgO) presented lower intrinsic activity in the SELOX reaction than the reducible oxides (e.g. $ZrO_2$, $CeO_2$, $TiO_2$, $Fe_2O_3$). The reducible oxides supply $O_2$ for the reaction, improving the activity and decreasing drastically its dependence on particle sizes. The facility of supplying oxygen in these materials occurs by the formation of superoxides ($O^{2-}$) on the neighboring particles. These oxygen species migrate to the surface or at the interface of the particles, reacting with CO adsorbed species on metallic sites [24,37,38]. The reducible supports are oxygen sources and therefore active phases. These oxygen species enhances the oxidation process either for CO conversion and $H_2$ oxidation.

The Mössbauer results may elucidate the particular role of the oxidation state of Fe in the mixed oxide and the interaction with the metal. The parameters showed that the catalysts reduced at 500 °C presented $Fe_3O_4$ in the structure, decreasing their content when the zirconium loading is increased. Besides, the $Fe_3O_4$ is less stoichiometric in the same direction. Therefore, the $Fe^{3+}$ ions at the surface may interact with $Pt^{\circ}$ at the interface, generating new sites, which enhances the CO and $H_2$ adsorption and the $H_2$ spillover to the support. According to Schubert et al. [36] these facts provoke the formation of superoxides ($O^{2-}$) at the neighboring particles, which promotes the formation of vacancies in the mixed oxide and facilitate the oxygen mobility, affecting the electronic structure [6] of the support and the metal. The results indicate that these oxides present different behaviors in the selective oxidation reaction due to the creation of new sites and vacancies depending of the iron content. For higher iron contents the CO adsorption is inhibited favoring the $H_2$ oxidation.

## 4. Conclusions

- XRD analysis showed that the iron oxide presented hexagonal α-$Fe_2O_3$ structure. The mixed oxides presented a solid solution of Fe–Zr for 25% iron content, while the mixed oxides with 50 and 75% iron content presented segregated oxides in the structure.
- TPR results showed that the addition of Pt favored the reduction of iron oxide at lower temperatures, probably due to the interaction at the metal surface interface. The degree of reduction of the mixed oxide containing 25% of iron was 94%. However, increasing iron loading, the degree of reduction lowered, confirming the presence of segregated phases on these mixed oxides.
- The TPD-feed profiles of $Pt/Fe_2O_3$ displayed only very small desorption of $CO_2$ and CO above 200 °C and not $H_2$ desorption. On the other hand, the TPD-feed profile of $Pt/Fe_{0.25}Zr_{0.75}O_2$ showed one large desorption peak of $CO_2$ at 195 °C, but not $H_2$ desorption.
- The TPD-feed profiles of the $Pt/Fe_{0.5}Zr_{0.5}O_2$ and $Pt/Fe_{0.75}Zr_{0.25}O_2$ catalysts, are completely different, displaying very small desorptions of CO and $CO_2$ but great $H_2$ desorption above 200 °C.
- Mössbauer results showed the presence of $Fe^{3+}$ diffusing into the lattice of zirconia in $Pt/Fe_{0.25}Zr_{0.75}O_2$(p), and the formation of an amorphous mixed oxide, in agreement with the XRD results, suggesting the formation of a solid solution.
- Catalytic tests for the selective oxidation of CO containing $H_2$ showed a maximum CO conversion at different temperatures after reaching total oxygen conversion. Results showed the following activity order: $Pt/Fe_2O_3(c) > Pt/Fe_{0.75}Zr_{0.25}O_2(c) > Pt/Fe_{0.25}Zr_{0.75}O_2(c) > Pt/ZrO_2$. The $Pt/Fe_{0.25}Zr_{0.75}O_2$(c) presented high selectivity (56%) at 90 °C and is 2-fold higher compared to the $Pt/Fe_2O_3$ and $Pt/ZrO_2$ catalyst. These results depend on the iron content. The CO conversion decreased drastically when the iron content in the mixed oxide is increased.

## Acknowledgments

CAPES, FINEP, MCT for the financial support and CNPq for the scholarship (R.S.).

## References

[1] N. Bion, F. Epron, M. Moreno, F. Mariño, D. Duprez, Top. Catal. 51 (2008) 76–88.
[2] H. Tanaka, M. Kuriyama, Y. Ishida, S.I. Ito, K. Tomishige, K. Kunimori, Appl. Catal. A: Gen. 343 (2008) 117–124.
[3] O. Pozdnyakova, D. Teschner, A. Wootsch, J. Kröhnert, B. Steinhauer, H. Sauer, L. Toth, F.C. Jentoft, A. Knop-Gericke, Z. Paál, R. Schlögl, J. Catal. 237 (2006) 17–28.
[4] S.Y. Chin, O.S. Alexeev, M.D. Amiridis, Appl. Catal. A: Gen. 286 (2005) 157–166.
[5] Y.F. Han, M.J. Kahlich, M. Kinne, R.J. Behm, Appl. Catal. B: Environ. 50 (2004) 209–218.
[6] G.J. Hutchings, M.S. Hall, A.F. Carley, P. Landon, B.E. Solsona, C.J. Kiely, A. Herzing, M. Makkee, J.A. Moulijn, A. Overweg, J.C. Fierro-Gonzalez, J. Guzman, B.C. Gates, J. Catal. 242 (2006) 71–81.
[7] F. Mariño, C. Descorme, D. Duprez, Appl. Catal. B: Environ. 58 (2005) 175–183.

[8] W. Liu, A. Sarofin, M. Flytzani-Stephanopoulos, Appl. Catal. B: Environ. 4 (1994) 167–186.
[9] Z. Wu, H. Zhu, Z. Qin, H. Wang, J. Ding, L. Huang, J. Wang, Fuel, in press.
[10] M. Hino, K. Arata, Catal. Lett. 36 (3–4) (1996) 125–128.
[11] J.C. Wu, D.S. Liu, A.N. Ko, Catal. Lett. 20 (1993) 191–201.
[12] K.D. Chen, Y.N. Fan, Z. Hu, Q. Yan, J. Solid State Chem. 121 (1996) 240–246.
[13] K.D. Chen, Y.N. Fan, Z. Hu, Q. Yan, Catal. Lett. 36 (1996) 139–144.
[14] S. Popovic, B. Grzeta, G. Stefanic, I. Czako-Nagy, S. Music, J. Alloys Compd. 241 (1996) 10–15.
[15] G. Stefanic, B. Grzeta, S. Music, Mater. Chem. Phys. 65 (2000) 216–221.
[16] K. Lagarec, D.G. Rancourt, "Mössbauer spectral analysis software". Version 1.0, Department of Physics University of Ottawa, 1998.
[17] S.G. Marchetti, J.F. Bengoa, M.V. Cagnoli, A.M. Alvarez, N.G. Gallegos, A.A. Yeramián, R.C. Mercader, Meas. Sci. Technol. 7 (1996) 758–762.
[18] A.K. Tripathi, V.S. Kamble, N.M. Gupta, J. Catal. 187 (1999) 332–342.
[19] J. Qiu, R. Yang, M. Li, N. Jiang, Mater. Res. Bull. 40 (2005) 1968–1975.
[20] A.S. de Menezes, C.M.R. Remédios, J.M. Sasaki, L.R.D. da Silva, J.C. Góes, P.M. Jardim, M.A.R. Miranda, J. Non-Cryst. Sol. 353 (2007) 1091–1094.
[21] W.M. Shaheen, Mater. Chem. Phys. 101 (2007) 182–190.
[22] G. Stefanic, B. Grzeta, K. Nomura, R. Trojko, S. Music, J. Alloys Compd. 327 (2001) 151–160.
[23] J.L. Ayastuy, M.P. González-Marcos, A. Gil-Rodríguez, J.R. González-Velasco, M.A. Gutiérrez-Ortiz, Catal. Today 116 (2006) 391–399.
[24] N.F.P. Ribeiro, F.M.T. Mendes, C.A.C. Perez, M.M.V.M. Souza, M. Schmal, Appl. Catal. A: Gen. 347 (2008) 62–71.
[25] M.O.G. Souza, E.B. Quadro, M.C. Rangel, Química Nova 21 (1998) 428–433.
[26] K. Chen, Y. Fan, Z. Hu, Q. Yan, J. Solid State Chem. 121 (1996) 240–246.
[27] P. Heidebrecht, V. Galvita, K. Sundmacher, Chem. Eng. Sci. 63 (2008) 4776–4788.
[28] H.-Y. Lin, Y.-W. Chen, C. Li, Thermochim. Acta 400 (2003) 61–67.
[29] G. Smit, N. Strukan, M.W.J. Crajé, K. Lázár, J. Mol. Catal. A: Chem. 252 (2006) 163–170.
[30] R.E. Vandenberghe, E. De Grave, C. Landuydt, L.H. Bowen, Hyperfine Interact. 53 (1990) 175–196.
[31] S. Mørup, H. Topsøe, Appl. Phys. 11 (1976) 63–66.
[32] G. Stefanic, S. Music, S. Popovic, K. Nomura, J. Mol. Struct. 480/481 (1999) 627–631.
[33] M.V. Mansilla, R.D. Zysler, C. Arciprete, M.I. Dimitrijewits, J.M. Greneche, J. Magn. Magn. Mater. 204 (1999) 29–35.
[34] A. Wootsch, C. Descorme, D. Duprez, J. Catal. 225 (2004) 259–266.
[35] C. Rossignol, S. Arrii, F. Morfin, L. Piccolo, V. Caps, J.-L. Rousset, J. Catal. 230 (2005) 476–483.
[36] M.M. Schubert, V. Plzak, J. Garche, R.J. Behm, Catal. Lett. 76 (2001) 143–150.
[37] H. Liu, A.I. Kozlov, A.P. Kozlova, T. Shido, K. Asakura, Y. Iwasawa, J. Catal. 185 (1999) 252–264.
[38] P. Konova, A. Naydenov, C. Venkov, D. Mehandjiev, D. Andreeva, T. Tabakova, J. Mol. Catal. A 213 (2004) 235–240.